공학석사학위논문

Experimental and numerical study of colloidal fouling on the patterned membrane surface

패턴형 분리막에서의 막오염에 대한 실험 및 수치해석 연구

2014년 8월

서울대학교 대학원

화학생물공학부

정 선 엽

Experimental and numerical study of colloidal fouling on the patterned membrane surface

패턴형 분리막에서의 막오염에 대한 실험 및 수치해석 연구

지도교수 **안 경 현**

이 논문을 공학석사학위논문으로 제출함
2014년 6월

서울대학교 대학원
화학생물공학부

정 선 엽

정선엽의 석사학위논문을 인준함
2014년 6월

위 원 장 _____ (인)

부위원장 _____ (인)

위 원 _____ (인)

Abstract

Experimental and numerical study of colloidal fouling on the patterned membrane surface

Jung, Seon Yeop
School of Chemical and Biological Engineering
The Graduate School
Seoul National University

In this study, microfiltration experiments were conducted to observe membrane fouling in the patterned membrane and they were compared to dynamics of suspended particles calculated from Brownian dynamics simulation. Patterned membranes were fabricated with the modified immersion precipitation method, and they were located in the microfiltration test cell. A monodisperse PMMA colloidal suspension was sonicated and used as the feed solution. After cross-flow microfiltration experiments, fouled surfaces of the patterned membranes were observed with scanning electron microscope (SEM). We could observe that colloidal fouling occurred readily in the valley region between the surface patterns in comparison to the apex region.

Brownian dynamics simulation was modified to be conducted with perturbed flow field near the patterned membrane which was calculated from the Navier-Stokes equations and continuity equations. Dynamics of colloidal particles were simulated in the case of PMMA colloidal suspensions, and they were affected by the flow characteristics near the patterned membrane surface. High shear stress distribution and flow separation were shown in this area, so fouling behavior could be explained with these flow characteristics. Colloidal fouling phenomena observed in the

experiment could be related to the particle dynamics calculated in the Brownian dynamics simulation.

Key words: microfiltration, membrane fouling, patterned membrane, Brownian dynamics simulation

Student Number: 2012-20976

Contents

Abstract.....i

List of Figures.....v

Chapter 1 Introduction.....1

1.1. Membrane fouling.....1

1.2. Patterned membranes.....3

Chapter 2 Experimental.....5

2.1. Materials.....5

2.2. Membrane fabrication.....5

2.3. Cross-flow microfiltration.....7

Chapter 3 Numerical Simulation.....10

3.1. Brownian dynamics simulation.....10

3.1.2. Langevin equation.....10

3.1.2. Interparticle force.....13

3.2. Simulation domain.....16

3.3. Boundary conditions.....19

Chapter 4 Result and Discussion.....24

4.1. Experimental.....24

4.1.1. Membrane characterization.....24

4.1.2. Observation of colloidal fouling.....26
4.2. Numerical simulation.....30
4.2.1. Mesh convergence.....30
4.2.2. Flow characteristics near the patterned membrane surface.....32
4.2.3. Fouling behavior on the patterned membrane.....34
4.2.4. Implication on biofouling in the patterned membrane.....39

Chapter 5 Conclusion.....40

Reference.....41

국문요약.....44

List of Figures

Figure 2.1. Schematic diagram of cross-flow microfiltration experiment.....9

Figure 3.1. DLVO potential between two identical PMMA particles.....15

Figure 3.2. Simulation domain and computational mesh.....18

Figure 3.3. Boundaries of simulation domain.....22

Figure 3.4. DLVO potential between a PMMA particle and membrane surface... 23

Figure 4.1. Cross section of patterned membrane surface.....25

Figure 4.2. Apex region of fouled patterned membrane surface. White spheres are deposited PMMA particles. (a) 5min, (b) 30min after the cross-flow microfiltration experiment.....28

Figure 4.3. Valley region of fouled patterned membrane surface. White spheres are deposited PMMA particles. (a) 5min, (b) 30min after the cross-flow microfiltration experiment.....29

Figure 4.4. Mesh convergence of overall wall shear stress.....31

Figure 4.5. Flow characteristics near the patterned membrane surface. (a) streamline, (b) velocity magnitude, and (c) shear stress distribution.....33

Figure 4.6. Snapshots of colloidal fouling on the patterned membrane surface of the apex region at dimensionless time (a) 1000, (b) 4000, (c) 7000.....35

Figure 4.7. Snapshots of colloidal fouling on the patterned membrane surface of the valley region at dimensionless time (a) 1000, (b) 4000, (c) 7000...36

Figure 4.8. Number of deposited colloidal particles per unit length counted in the area between surface patterns.....38

Chapter 1 Introduction

1.1. Membrane fouling

As the world has been developed rapidly, our environments have been damaged and destroyed. Global average ecological footprint which is a measure of human demand on the ecosystem of the earth is 1.5 in 2012. [1, 2] This means it takes 1.5 years to reproduce what we use in a year. One of the major environmental crises that threaten our human civilization is inadequate access to clean water. [3] More than 1.2 billion people suffer from polluted water, and 15 million children are passed away from unsafe water every year. [4] Also waste water problems are spreading worldwide with accelerated climate change, and they are significant challenges of human civilization.

In this context, it is spotlighted to develop stainable, energy efficient water treatment technologies. Formerly, large scale of water purification treatment plant treated polluted water with sanitation facilities demanding huge energy consumption and a lot of chemical agents to obtain clean water. Recently, however, membrane technologies are applied to the waste-water treatment to purify waste water with low cost and energy consumption. Membrane technologies are classified into microfiltration (MF), ultrafiltration (UF), nanofiltration (NF), reverse osmosis (RO) by the pore size, and it is possible to compose an integrated membrane systems (IMS) with several types of membranes to purify waste water systematically. [5] Membrane technology is one of the core environmental technologies to solve water problems with less chemical treatment and more flexible operations of the water purification process.

However, membrane technology has a critical drawback. When membrane technologies are used in the separation process, suspended particles and organic or inorganic substances are clogged on the surface or in the pore of the membrane to decrease processed water flux and to lead inferior quality of the purified water. This phenomenon is called “membrane fouling” which is classified into inorganic fouling/scaling, organic fouling, particulate/colloidal fouling, biofouling. [6] These could occur simultaneously and affect each other. Therefore a wide range of technologies to mitigate membrane fouling have been developed such as back-washing, membrane relaxation, back pulsing, chemical enhanced backwash, chemical cleaning, and so forth.

1.2. Patterned membrane

It has been much easier to control surface morphology with the aid of the recent development in micro-fabrication technologies such as photolithography, forced ion-beam lithography, EHD printing, and micro molding. Phase separation micro molding (PSum) which is the combination of micro molding and phase inversion to method is reported as a unique pattern transfer technique to fabricate a micro-structured surface with porous network. [7] It has been well reported that membranes with micro-patterned surface have anti-fouling properties, so micro-structured surface morphology is expected to increase the sustainability of membranes. [8, 9] Çulfaz [10, 11] fabricated patterned hollow fiber membrane with this technology, and she reported increased pure water flux and improved anti-fouling properties. Won [12] modified this technology to form a dense layer on the side of surface patterns and prepare patterned membranes in the form of sheets.

In recent years, anti-fouling properties and correlation between fouling and pattern topology of the patterned membrane have been actively discussed and studied. Won [12] fabricated patterned membranes with various shapes of surface patterns, and analyzed membrane fouling in patterned membranes. On the other hand, Lee [13] conducted numerical simulation to understand flow characteristics near the patterned membrane surface. He reported that high wall shear stress was distributed near the upper region of the valley area and vortex region was increased with flow rate. From these studies anti-fouling properties are thought to have close relationship with flow characteristics which are varied with shapes of surface patterns and flow conditions.

In this study, cross-flow microfiltration experiments with patterned membranes and model feed solution were performed and Brownian dynamics simulation was

conducted to analyze fouling phenomena on patterned membranes. To capture the dynamics of buoyant particles near the patterned membrane surface, mono-disperse spherical PMMA particle suspension was used in the experiment. Also dynamics of suspended particles were calculated with distorted flow field, interparticle forces, and thermal random motions by Brownian dynamics simulation. From the results of this study, flow characteristics which were induced by the topological properties of patterned membrane were analyzed with fouling phenomena. Advanced patterned membranes with anti-fouling properties are expected to be designed with the aid of the results from this study.

Chapter 2 Experimental

2.1. Materials

Patterned membranes used in this study were fabricated by the modified immersion precipitation method which was reported by Won et al. [12]. Polydimethylsiloxane (PDMS, Sylgard 184A, Dow Corning, USA) and curing agent (Sylgard 184B, Dow Corning, USA) were purchased and used to synthesize the soft replica mold. To replicate surface patterns, a metal master mold with micro-machined 400um x 100um prism patterns on the surface was utilized. Polyvinylidene fluoride (PVDF, Sigma Aldrich, Korea), dimethyl formamide (DMF, Sigma Aldrich, Korea), and acetone (Sigma Aldrich, Korea) were used to fabricate patterned membranes with the replica mold by phase-inversion method. PMMA particles which have average diameter of 1.3um was used in the cross-flow microfiltration experiment.

2.2. Membrane fabrication

Prism patterns on the master mold were transferred to the membrane surface with the procedure as follows. A master mold which has micro-machined 400um x 100um surface prism patterns was obtained. PDMS was mixed with the curing agent (Sylgard 184B) in a ratio of 10:1, and this mixture was poured onto the master mold. It was cured for 2h at 60℃ to obtain PDMS replica mold with surface patterns which had transferred from the master mold. PDMS was chosen to fabricate the replica mold, because it is easily cured and has resistance to organic solution, which provided ideal condition for phase inversion.

PVDF was used to construct the patterned membranes. PVDF pellets were poured into the mixture of DMF and acetone, and they were dissolved with magnetic stirrer for 6 h at 60°C. PVDF mixture obtained from this procedure could be precipitated easily with the contact of water in room temperature. This PVDF mixture was carefully coated onto the PDMS replica mold. Non-wooven fabric was attached on the side of support layer to avoid the formation of dense layer in this side, and phase-inversion was induced in the coagulation bath filled with deionized water. After 6 to 10 h of coagulation, the PVDF patterned membrane was separated from the PDMS replica mold. From this procedure the patterned membrane was obtained and remained wet to be used in the cross-flow microfiltration experiment.

2.3. Cross-flow microfiltration

Cross-flow microfiltration experiments with model feed solution was performed to understand dynamics of buoyant particles near the patterned membrane surface. In this study, monodisperse spherical PMMA particle suspension was used as feed solution to perform cross-flow microfiltration experiment. PMMA particles used in this study had diameter of 1.3um.

PMMA particles were obtained in the form of powder and they were sonicated for 30 minutes to achieve well-dispersed state in deionized (DI) water. 0.001 vol% (10ppm) PMMA particle suspension was prepared and pumped to the microfiltration test cell in which the patterned membrane was located. A peristaltic pump (Masterflex, USA) was used in this experiment to generate constant flux, but pulsation was also induced by the motion of the pump. To avoid the disturbance from the pulsation, a flow dampener was inserted between the pump and the test cell to make a smoother flow. A pressure gauge was connected and the flow through retentate and permeate line was re-circulated to the feed solution. A valve was inserted in the retentate line to control the pressure loaded in the test cell to obtain the desired permeation flux.

If patterned membranes were used immediately after fabrication, the porous network of them could be deformed by the flow. So membrane compaction was performed for 1 h with deionized water before each microfiltration experiments. Flow rates of rententate and permeate line were set to be 56ml/min and 2ml/min each. Surface area of the patterned membrane was 10.23cm^2 in consideration of surface roughness and the membrane was located in the test cell which was 2mm in height, 15mm in width, and 61mm in length. Flow rate assigned in this experiment was less than the range of conventional operation of membrane separation process where flow

instability or transient flow could be induced. It was thought to be difficult to compare the results from an experiment with rapid flow with Brownian dynamics simulation which require flow condition slower than that of conventional operation. So, we conducted experiment in a slow flow condition to analyze dynamics of particles calculated from numerical simulation with the flow characteristics near the patterned membrane surface.

On the other hand, scanning electron microscope (SEM, JSM-6701F, Jeol, USA) was used to observe colloidal fouling on the patterned membrane surface from cross-flow microfiltration process with time. Fouled membranes after 5 minutes and 30 minutes from the initiation of the experiments were observed by SEM. Samples used in SEM imaging had been dried for a day, and segments of them were sampled in the center region of the membrane where the fidelity of surface patterns was high. Experiments were repeated two times to check the reproducibility.

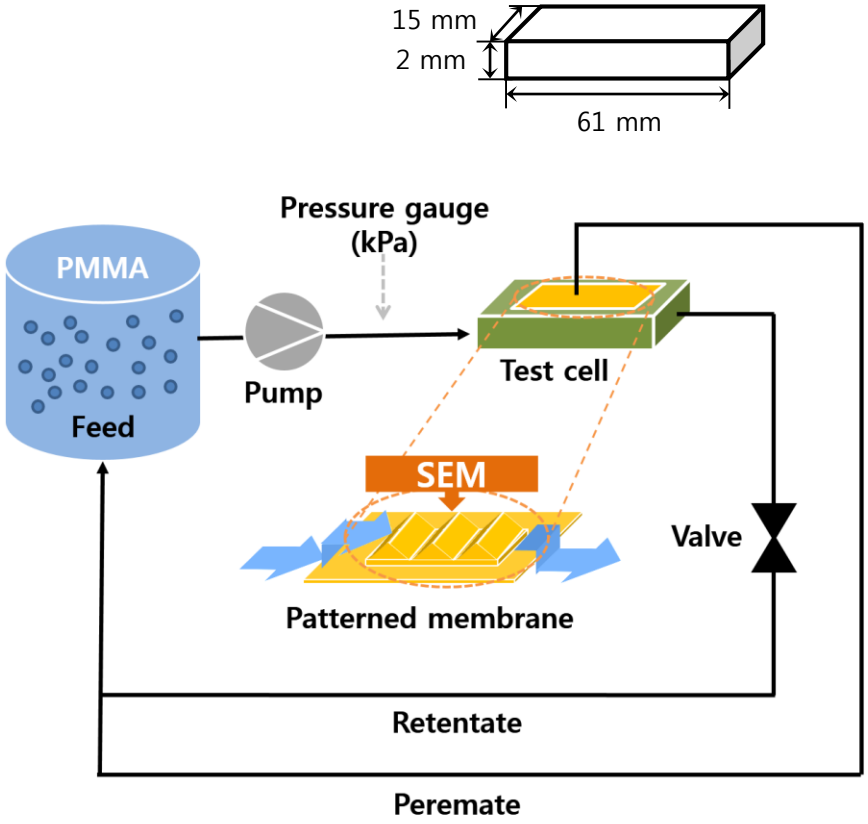

Figure 2.1. Schematic diagram of cross-flow microfiltration experiment.

Chapter 3 Numerical Simulation

3.1. Brownian dynamics simulation

Suspended colloidal particles in a fluid medium are continuously collided with fluid molecules to move randomly, these motions are called Brownian random motions. In general, it is impossible to consider all the collisions between suspended particles and fluid molecules, so fluid molecules are considered to be continuum and the Brownian motions induced from the collisions are treated as stochastic motions. [14] Brownian dynamics simulation could capture the motion of suspended particles with Brownian motion considered as a stochastic force.

3.1.1. Langevin equation

The motion of Brownian particles could be calculated from hydrodynamic force, interparticle force, and Brownian random force. It is described by Langevin equation:

$$m\frac{d\mathbf{v}_i}{dt} = \mathbf{F}_i^H + \mathbf{F}_i^P + \mathbf{F}_i^B \qquad (1)$$

in which m is the mass of a particle, v the particle velocity, F^H the hydrodynamic force exerted by suspending media, F^P the force exerted by the surrounding particles. If the colloidal suspension is very dilute and complex hydrodynamic interactions are neglected, F^H could be described as Stokes drag force. When the force exerted on a

particle is assumed to be constant in a short time interval, the equation below could be obtained.

$$0 = -\zeta(\mathbf{v}_i - \mathbf{v}_i^{\infty}) + \mathbf{F}_i^P + \mathbf{F}_i^B \tag{2}$$

where ζ is the Stokes drag coefficient, $\mathbf{v}_i$ the particle velocity, $\mathbf{v}_i^{\infty}$ the velocity of surrounding medium. If $\mathbf{F}_i^B$ is treated as a random variable, motion of a particle could be calculated as follows.

$$\mathbf{v}_i = \frac{d\mathbf{r}_i}{dt} = \mathbf{v}_i^{\infty} + \frac{1}{\zeta}(\mathbf{F}_i^P + \mathbf{F}_i^B) \tag{3}$$

$$< \mathbf{F}_t^B >= 0\,, \quad < \mathbf{F}_t^B \mathbf{F}_{t'}^B >= 2\zeta k_B T \delta(t - t')\mathbf{I} \tag{4}$$

$$d\mathbf{r}_i = \left(\mathbf{v}_i^{\infty} + \frac{1}{\zeta}\mathbf{F}_i^P \right) dt + \sqrt{\frac{2k_B T}{\zeta}}\, d\mathbf{W}_t \tag{5}$$

$$\left(< d\mathbf{W}_t >= 0, < d\mathbf{W}_t d\mathbf{W}_{t'} >= \delta(t - t')\mathbf{I}dt \right) \tag{6}$$

in which $d\mathbf{W}_t$ is the unit vector of Brownian random force, k_B the Boltzmann constant. And interparticle force ($\mathbf{F}_i^P$) is calculated from DLVO (Derjaguin-Landau-Verwey-Overbeek) potential to describe interactions between PMMA colloidal particles in more realistic way. Non-dimensionalization is performed with characteristic values below to obtain the final equation.

$$
\begin{aligned}
&\textit{characteristic length} \;:\; l_c = a = 0.65\mu m \\
&\textit{characteristic time} \;:\; t_c = \frac{a^2}{D} = \frac{6\pi\mu a^3}{k_B T} = 1.26s \\
&\textit{characteristic force} \;:\; f_s = \frac{k_B T}{a} = 6.33fN
\end{aligned}
\tag{7}
$$

$$
d\mathbf{r}_i^* = \left[\mathbf{v}^{\infty *}(\mathbf{r}_i^*) + \mathbf{F}_i^{P*} \right] dt^* + \sqrt{2} d\mathbf{W}_t^* \tag{8}
$$

Brownian dynamic simulation was performed with the equation above until dimensionless time reach the value of 10,000. Computational time step was assigned to be 10^{-4}, so 1×10^8 times calculations were conducted.

3.1.2. Interparticle force

We wanted to describe motions of suspended PMMA particles, so DLVO (Derjaguin-Landau-Verwey-Overbeek) theory was used to calculate interparticle forces. Van der Waals interaction and electrostatic double layer interaction are summed up to describe DLVO potential:

$$V = V_A + V_R \tag{9}$$

in which V_A is the attractive interaction, V_R the repulsive interaction. They are evaluated as below.

$$V_A = -\frac{A_H}{12}\left[\frac{d^2}{H(H+2d)} + \frac{d^2}{(H+d)^2} + 2\ln\left(\frac{H(H+2d)}{(H+d)^2}\right)\right] \tag{10}$$

$$V_R = \frac{32\pi\varepsilon a k^2 T^2 \gamma^2}{z^2 e^2}\exp(-\kappa H) \quad \left(\gamma = \frac{\exp[ze\psi_d / 2kT]-1}{\exp[ze\psi_d / 2kT]+1}\right) \tag{11}$$

where H is the shortest distance between the two particles, d the diameter of particles, ε the permittivity of the medium, k the Boltzmann constant, κ the inversion of the Debye-Hückel screening length, a the diameter of the particles, z the counter-ion charge, ψ_d the stern potential, and A_H the Hamaker constant.

Measured value of zeta potential of PMMA particle in the experiment was used in this simulation. This value was measured in 0.001M NaCl solution, and it was obtained to be -20.98mV at pH 7. Hamaker constant of a PMMA particle in water was obtained from the preceding study. [15]

$$A_{131} = \left(\sqrt{A_{11}} - \sqrt{A_{33}}\right)^2, \quad A_{33}(water) = 3.7 \times 10^{-20}$$
$$A_{131} = 1.53 \times 10^{-20} J \tag{12}$$

Interparticle force could be obtained from the DLVO potential with the equation below.

$$F = -\nabla V = -\frac{dV}{dr} \tag{13}$$

Interparticle force calculated from DLVO potential was plotted in Figure 3.1. Negative value of dimensionless force means attractive force and positive value of it means repulsive force. In this case, PMMA particles are weakly-aggregating particles. To avoid numerical artifact with too strong repulsive force, cutoff distance was assigned at the position where dimensionless force is more than 100. When the distance between particles is less than this cutoff distance, the interparticle force is bounded to be 100. With this amount of force, unphysical motions of a particle could be avoided by preventing movement of a particle more than 1% of the radius of it in a time step.

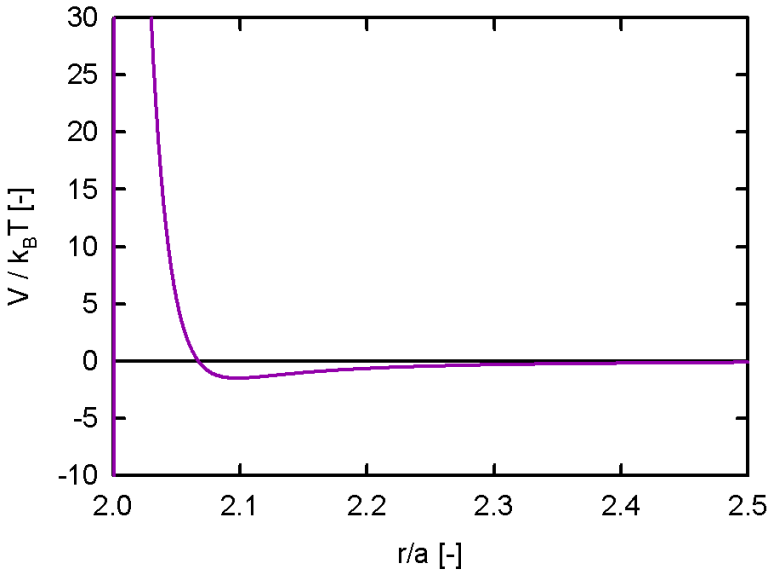

Figure 3.1. DLVO potential between two identical PMMA particles.

3.2. Simulation domain

In the experiment, patterned membrane had 400um x 100um prism-shaped surface patterns, and the width of the test cell where feed suspension enters is 15mm, which is long enough to neglect the z-directional flow. So we decided to solve the flow field in 2D without consideration of z-directional flow. Simulation domain was generated to have 6000μm width and 2000μm height with geometry of surface patterns. From the solution of the governing equation in the simulation domain, flow field was obtained.

$$-\rho(\mathbf{u}\cdot\nabla)\mathbf{u} = -\nabla p + \mu\nabla^2\mathbf{u} \tag{14}$$

$$\nabla\cdot\mathbf{u} = 0 \tag{15}$$

in which ρ is the fluid density, $\mathbf{u}$ the velocity vector of fluid, p the pressure, μ the fluid viscosity. Fluid considered in this simulation could be treated as pure water because the PMMA particle suspension used in the experiment was very dilute. Physical properties of pure water were used in the simulation, $\rho = 1000\,kg/m^3$, $\mu = 1\times10^{-3}\,Pa\cdot s$.

COMSOL Multiphysics 3.2 (Comsol inc., USA) was used in this calculation, and 14,175 elements were generated and used. For more accurate calculation, nodal points were generated more in the apex and valley region of the membrane surface.

Meanwhile, we set the "sub-domain" near the membrane surface to conduct Brownian dynamics simulation with reduced computational cost. Sub-domain was

set from the flow inlet with the assumption of constant concentration of colloidal particle in this boundary. To observe particle deposition phenomena, width of the sub-domain was assigned as six times the width of surface pattern. And height of the sub-domain was set from the membrane surface to the position where disturbed flow field is diminished enough.

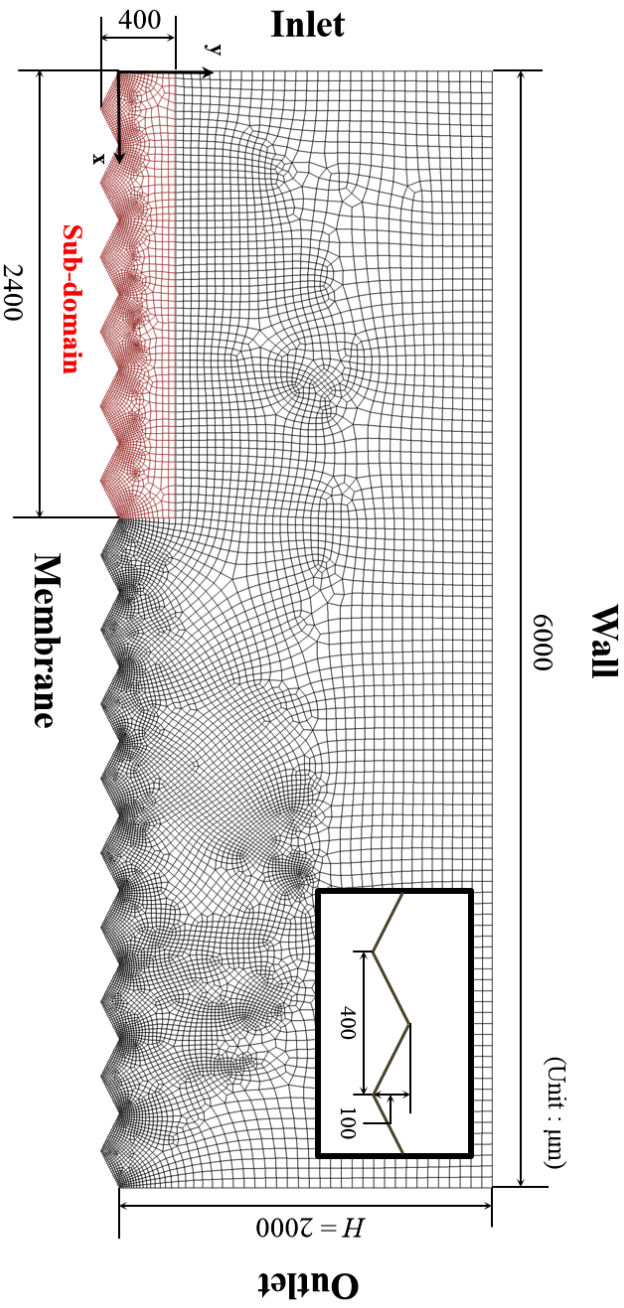

Figure 3.2. Simulation domain and computational mesh.

3.3. Boundary conditions

Boundary conditions were set to obtain flow field in the simulation domain as follows. (Figure 3.3.) Each boundaries of the simulation domain were named as B1~B4, and each boundaries of the sub-domain where Brownian dynamics simulation was performed were assigned as SB1 ~ SB4.

For the flow boundary conditions, fully developed parabolic velocity profile was imposed at the B1 boundary, the flow inlet.

$$u_x(y) = 4u_{max}\, y(H - y)/H^2 \tag{16}$$

in which u_{max} is the maximum velocity of inlet and set to be 1mm/s, and H the channel height, 2000um. This flow condition was slower than in the experiment. With rapid flow condition, unphysical overlapping phenomena readily occurred, so computational time step should be decreased to avoid this numerical artifact. Therefore more advanced algorithm is required to perform the simulation with similar flow velocity in the experiment. In this simulation, we intended to observe fouling on the membrane with this slower flow condition than in the experiment where important flow characteristics near the patterned membrane surface such as flow separation and high shear stress distribution in the apex region of the membrane surface exist. So we focused on this point.

At B2 boundary, which is the membrane surface, constant permeate velocity which had the value of 1/1000 u_{max} was assigned with normal direction to the membrane surface to consider only the averaged effect of permeate flow. At the B3 boundary, the wall of test cell, no-slip boundary condition was applied. At the B4 boundary, the

flow inlet, pressure was set to be zero which is a general boundary condition for pressure-driven flow.

Boundary conditions for particles calculated by Brownian dynamics simulation were assigned at the boundaries of the sub-domain. At SB1 boundary, where colloidal particles were ejected into the simulation domain, particles were generated with constant concentration along with y-direction.

At SB2 boundary, the part of membrane surface, interactions between a particle and the membrane were considered with DLVO potential which was evaluated between a spherical particle and an infinite flat plate. [16]

$$V = V_A + V_R \tag{17}$$

$$V_A = -\frac{A_H}{12}\left[\frac{d}{H} + \frac{d}{H+d} + \ln\left(\frac{H}{H+d}\right)\right] \tag{18}$$

$$V_R = \frac{64\pi\varepsilon a k^2 T^2 \gamma^2}{z^2 e^2}\exp(-\kappa H) \tag{19}$$

where, H is the shortest distance between particle and the plat plate.

Hamaker constant of a PMMA particle with PVDF in water was calculated. Hamaker constant of PVDF could be obtained from the research of J.W. Goodwin [17].

$$A_{132} = \left(\sqrt{A_{11}} - \sqrt{A_{33}}\right)\left(\sqrt{A_{22}} - \sqrt{A_{33}}\right), \quad A_{22}(PVDF) = 5.6\times10^{-20}$$
$$A_{132} = 5.49\times10^{-21} \tag{20}$$

Force between a particle and the surface of the membrane was plotted in Figure 3.4. Mainly, a particle feels attractive force from the membrane and it feels repulsive force when the distance between the center of the particle and the membrane surface is less than 1.07 times the radius of it.

When a particle moves across through SB3 and SB4 boundaries, they were excluded from the calculation. So calculation of interparticle forces was performed only in the sub-domain to observe colloidal fouling with reduced computational costs.

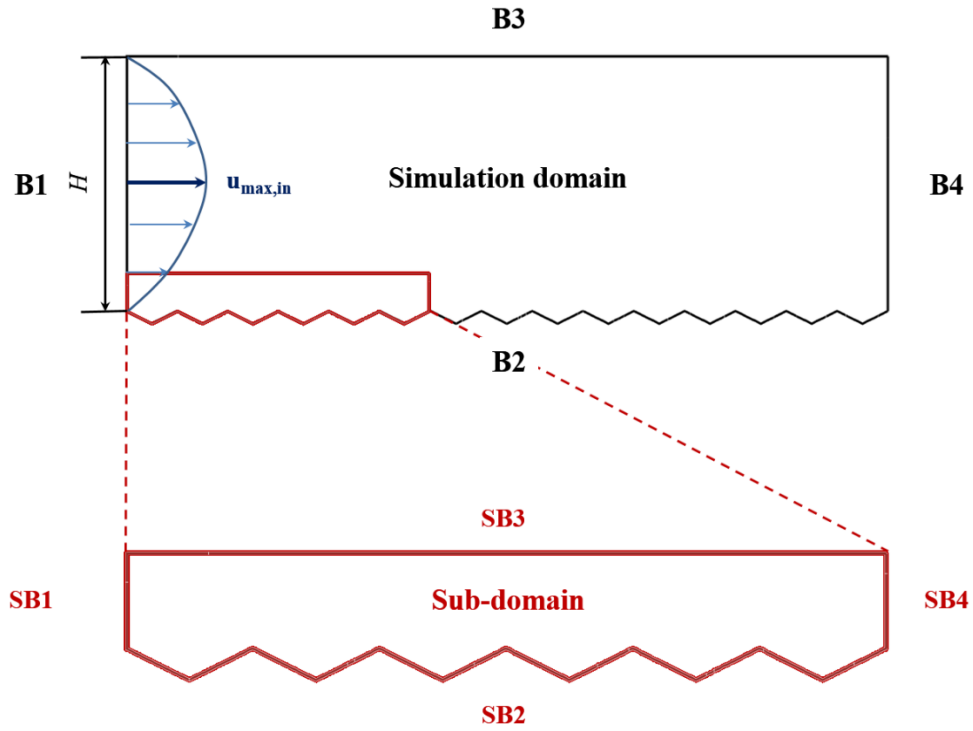

Figure 3.3. Boundaries of simulation domain.

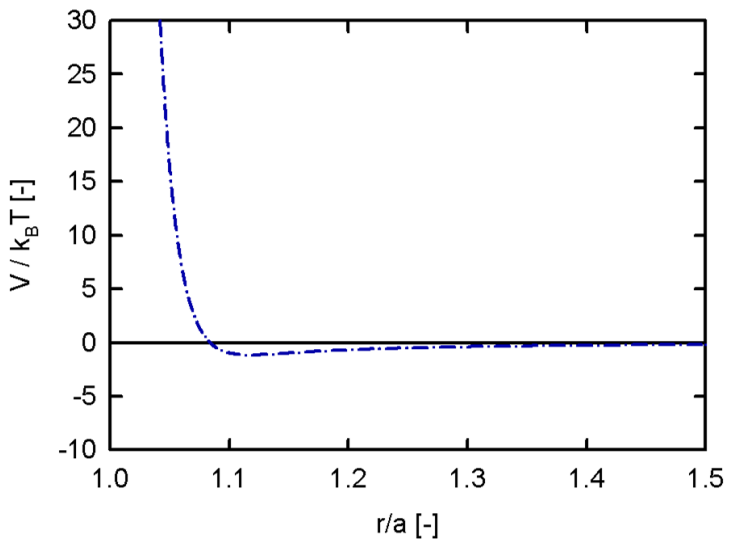

Figure 3.4. DLVO potential between a PMMA particle and membrane surface.

Chapter 4 Result and Discussion

4.1. Experimental

4.1.1. Membrane characterization

Through the modified immersion precipitation method, PVDF patterned membrane were fabricated onto the PDMS replica mold which had 400um x 100um prism surface patterns. To see the fidelity of the surface pattern on the PVDF patterned membrane, cross-section of the membrane surface which was quick-frozen with liquid nitrogen was observed with scanning electron microscope (SEM). (Figure 4.1) Surface patterns were transferred effectively through two-fold pattern transfer process, and the geometrical difference of the apex region and the valley region were obviously shown.

A dense skin layer could be formed on the side of surface patterns with modified immersion precipitation method to be used in microfiltration experiments. PVDF patterned membrane prepared with this process had mean pore size of 0.9um, which could be classified to microfiltration (MF) membrane, and it was reported to show around 20% increase in the pure water flux (PWF) in comparison to the flat membrane. [12]

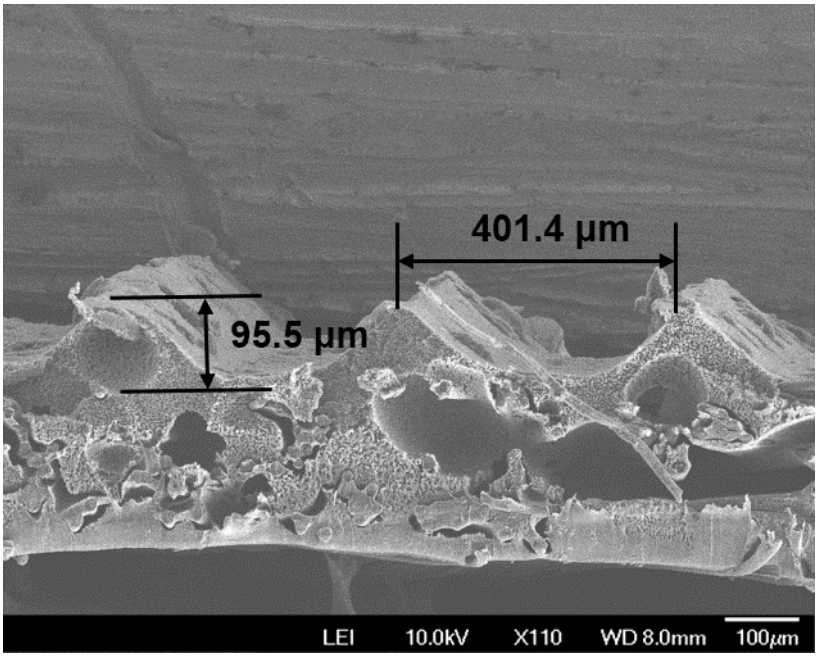

Figure 4.1. Cross section of patterned membrane surface.

4.1.2. Observation of colloidal fouling

Lab-scale cross-flow microfiltration experiments were performed to observe fouling phenomena on the patterned membrane. PMMA particle suspension were pumped into the microfiltration module in which the patterned membrane was located, and fouled surface of the patterned membrane was observed in top view with scanning electron microscope (SEM). SEM images were taken from the the apex region and valley region of the patterned membrane surface. (Figure 4.2, 4.3) Contrast of each images were enhanced up to 6-70% to observe the location of fouled particles obviously. In each images, white spheres represent PMMA particles and black area represents the membrane surface. The vertical lines in each images of the apex region are the peak of the surface patterns.

Figure 4.2 shows colloidal fouling in the apex region. After 5 minutes from the initiation of the microfiltration experiment, few particles were deposited, and they were started to be located on the membrane at a short distance from the peak of the surface pattern. After 30 minutes, more particles were deposited in this region. Non-fouled surface of the membrane was shown around the peak, which showed colloidal fouling in this region was mitigated. More particles were shown to be fouled toward the valley region than the apex region.

In the valley region, we could not observe mitigation of colloidal fouling. (Figure 4.3) As time proceeded, the number of fouled PMMA particles gradually increased, and they were deposited to cover the whole area of the membrane surface in the valley region. From this result, we could decide that colloidal fouling occurred more in the valley region rather than in the apex region, and fouling was mitigated in the apex

region. This could be related to the flow characteristics near the pattered membrane surface.

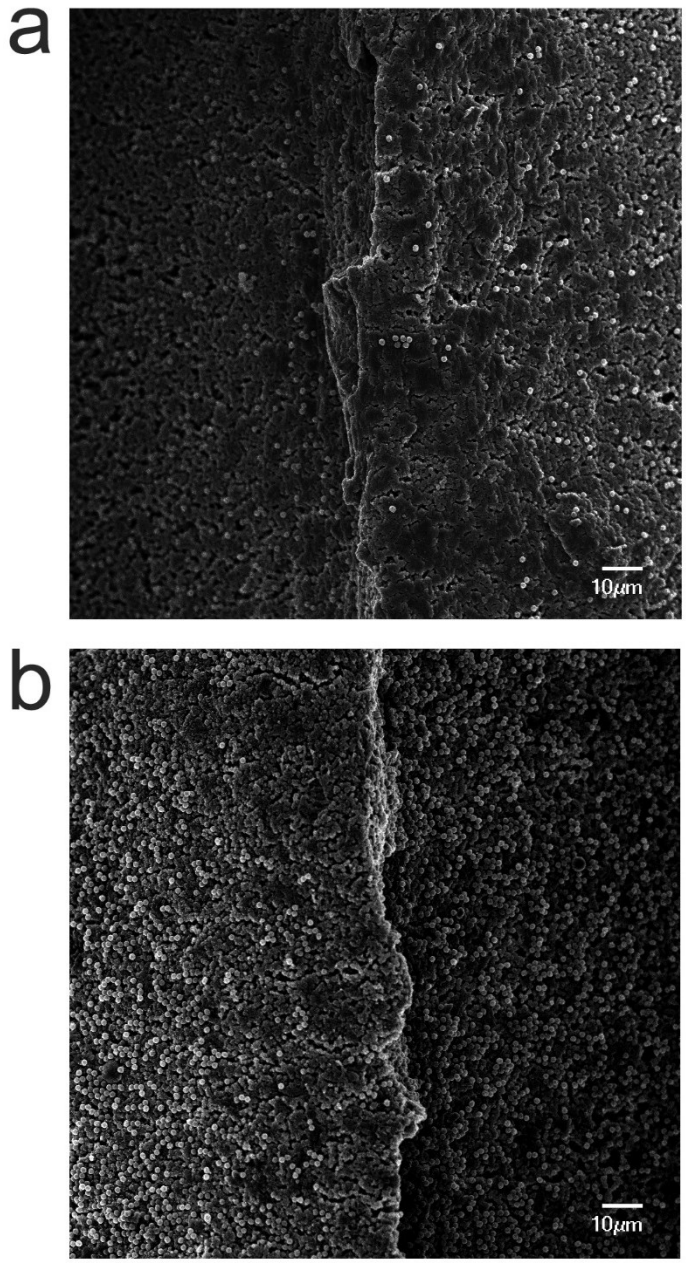

Figure 4.2. Apex region of fouled patterned membrane surface. White spheres are deposited PMMA particles. (a) 5min, (b) 30min after the cross-flow microfiltration experiment.

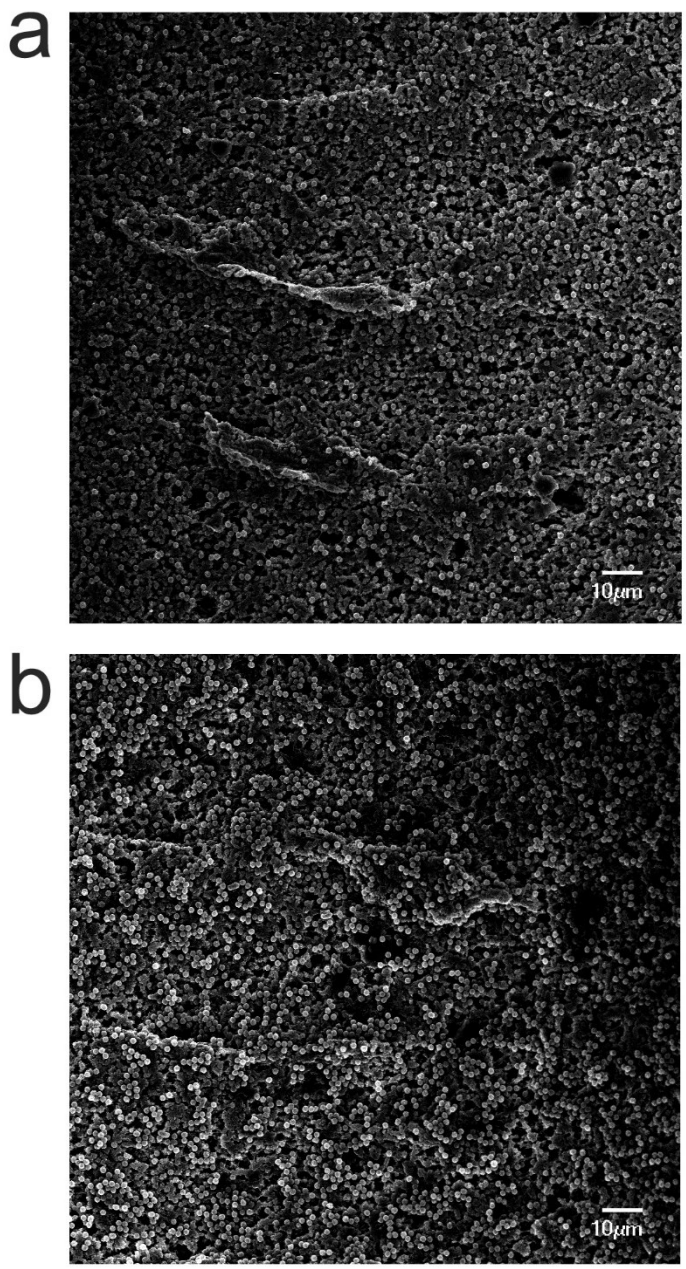

Figure 4.3. Valley region of fouled patterned membrane surface. White spheres are deposited PMMA particles. (a) 5min, (b) 30min after the cross-flow microfiltration experiment.

4.2. Numerical simulation

4.2.1. Mesh convergence

We generated computational meshes with free quadrature elements before conducting Brownian dynamics simulation. COMSOL Multiphysics 3.2 (Comsol inc., USA), a commercial CFD software, was used for mesh generation and calculation of the discretized governing equations. More nodal points were assigned near the apex region and the valley region because of the sharp geometry in these regions. To find the optimized number of elements for the simulation (NOE), mesh convergence was checked. We manipulate the number of nodal points at the boundary of membrane surface to generate five sets of computational meshes which are composed of 5,710, 8,581, 14,175, 17,017, and 22,250 elements each. And the overall wall shear stress values were calculated to see the mesh convergence. There were no significant variations in the value of wall shear stress from the number of elements, but we could observe that the converged value of the wall shear stress was obtained with more than 14,175 elements. Therefore, we used 14,175 elements to conduct numerical simulation with accuracy and efficiency.

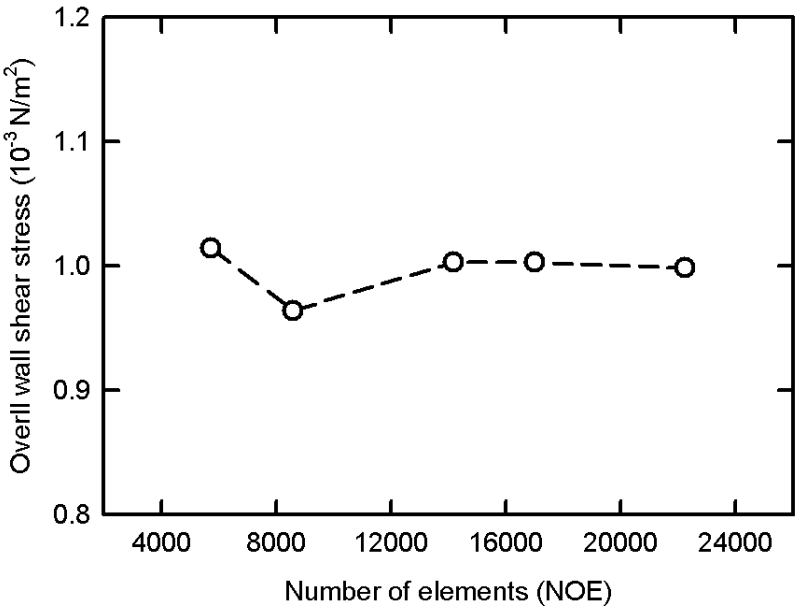

Figure 4.4. Mesh convergence of overall wall shear stress.

4.2.2. Flow characteristics near the patterned membrane surface

From the mesh convergence test, we could use optimized computational meshes to obtain the flow field near the patterned membrane surface. (Figure 4.5) Flow field around the surface patterns were visualized with perturbed streamline.

Streamline near the surface patterns showed distorted flow behavior, and permeation flux normal out to the membrane surface could be also found. This perturbation was diminished at far distance from the membrane surface. Therefore, dynamics of colloidal particles were analyzed near the patterned membrane surface with perturbed flow field.

Between the surface patterns, stagnant flow zone was formed. Flow velocity in this region was 0 ~ 0.1mm/s, which was less than 1/10 of maximum velocity. This was caused by the presence of surface patterns which induced flow separation with rapid bulk flow. When particles moved into this stagnant zone, they had little chance to be swept to the bulk flow and were easily deposited on the membrane surface.

Also, we could observe high wall shear stress in the apex region of the surface patterns. [13] Shear stress in the apex region showed three times the value of overall wall shear stress ($1\times10^{-3} N/m^2$). So when particles were deposited in this region, they were likely to be detached from the membrane surface by the influence of high shear force.

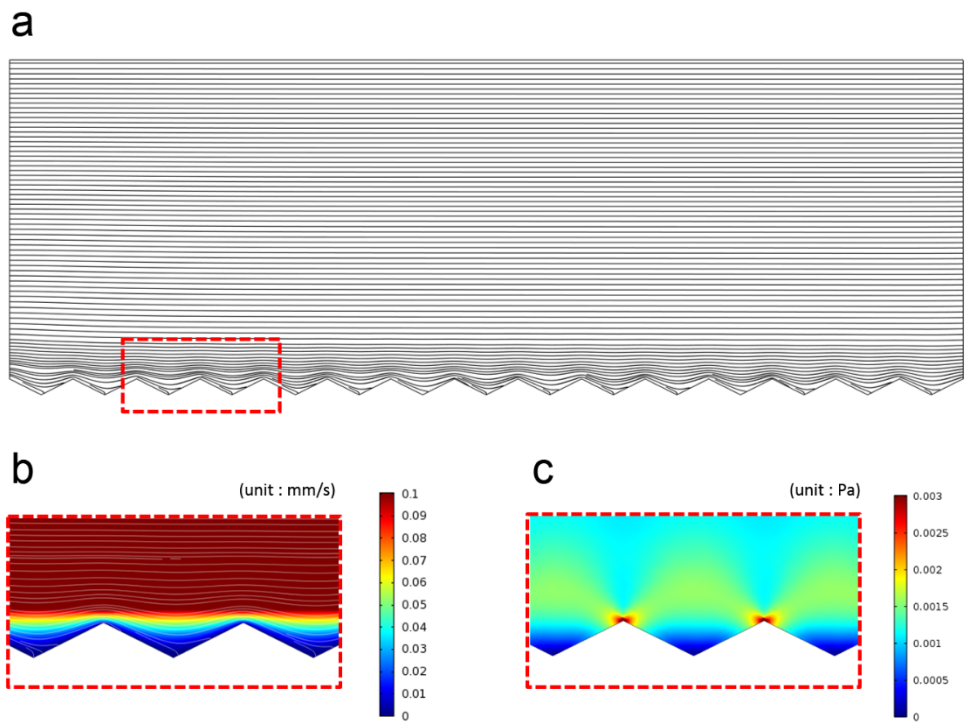

Figure 4.5. Flow characteristics near the patterned membrane surface.

(a) streamline, (b) velocity magnitude, and (c) shear stress distribution.

4.2.3. Fouling behavior on the patterned membrane

Brownian dynamics simulation was conducted to observe dynamics of PMMA particle suspension in the cross-flow microfiltration. Particles were deposited on the patterned membrane surface, and they showed different fouling phenomena in comparison to fouling occurred in a non-patterned membrane. This was thought to be induced by topological properties of the patterned membrane.

Figure 4.7 shows colloidal fouling in the apex region. At dimensionless time 1,000, few particles were deposited and uncovered surface of the membrane was shown. A number of particles were pumped into the simulation domain and they were contacted to the membrane surface or deposited onto the fouled particles, but they were swept easily by the influence of rapid bulk flow. The number of deposited particles on the membrane was reluctant to be increased even at dimensionless time 4,000 and 7,000.

This trend was also observed in the cross-flow microfiltration experiment. In the experiment, there were uncovered membrane surfaces in the apex region with small number of deposited particles, and this was thought to be related with flow characteristics. High shear stress distribution was observed in this region, so deposited particles could be washed away by the mainstream flow.

Colloidal fouling in the valley region could be shown in the figure 4.8. More particles were deposited in this region with time. Dynamics of particles in this region were very slow in the Brownian dynamics simulation because of stagnant zone formed in this area. Also, particles were affected by permeation flux and attractive DLVO forces from the membrane, so a number of particles were deposited onto the membrane surface. And they had little chance to be affected by the rapid bulk flow, and kept their place on the membrane surface.

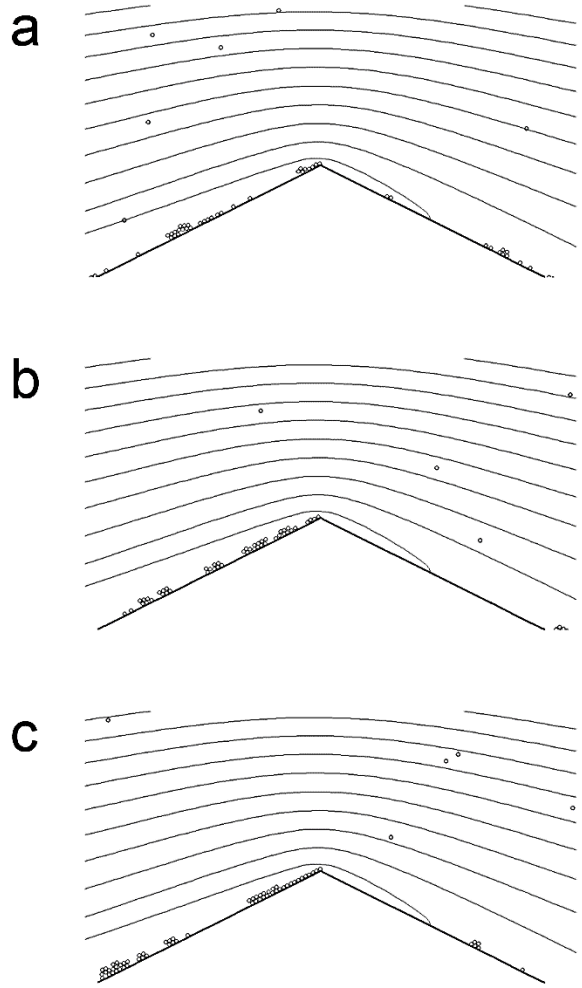

Figure 4.6. Snapshots of colloidal fouling on the patterned membrane surface of the apex region at dimensionless time (a) 1000, (b) 4000, (c) 7000.

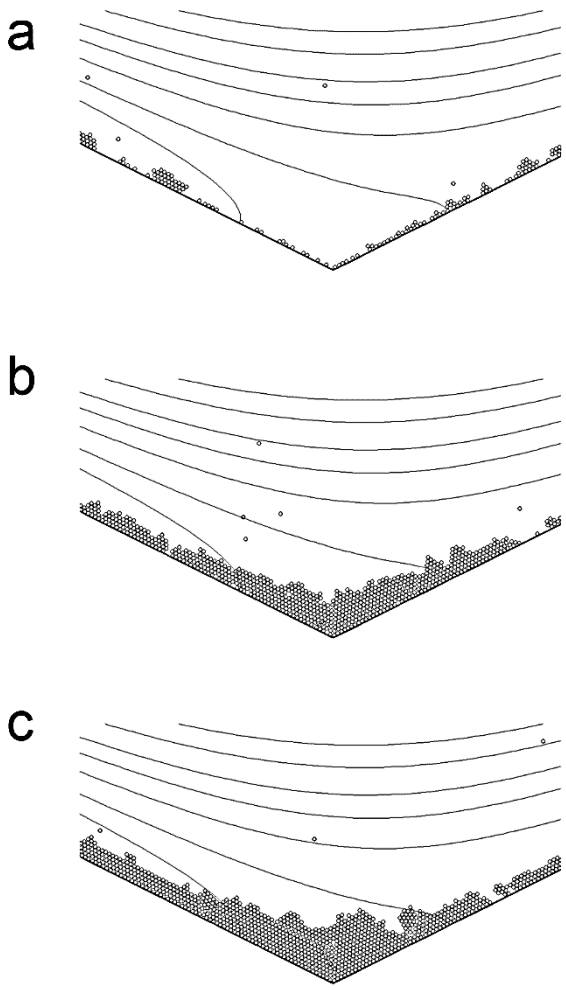

Figure 4.7. Snapshots of colloidal fouling on the patterned membrane surface of the valley region at dimensionless time (a) 1000, (b) 4000, (c) 7000.

Figure 4.9 shows the number of deposited colloidal particles per unit length. The area between surface patterns was divided into two region (the apex region and the valley region) to see the difference in the number of deposited particles. Because we calculated interparticle force between particles with DLVO potential, we could determine whether a particle is deposited or not through the distance from a contacted particle with the membrane surface.

If the value of interparticle force evaluated from DLVO potential is zero, a particle keeps in place because the attractive force and repulsive force have the same value. Equilibrium distance of particle-particle interaction was calculated to be 2.06 times the radius of a particle and that of particle-wall interaction was 1.07 times the radius of a particle. So, if the distance between a particle and the membrane is less than 1.07 times the radius of a particle, the particle experiences repulsive force from the membrane but it is also dragged to the membrane surface because of the presence of permeation. Therefore, a particle was determined to be contacted and counted to be fouled when it is closer than 1.07 times the radius of a particle to the membrane surface. And if the distance between the contacted particle and other particles is less than 2.06 times the radius of a particle, these particles were counted to be fouled on the membrane surface.

It was clearly shown that particles were reluctant to be fouled in the apex region, while deep foulant layer was formed in the valley region. And the number of deposited particles per unit length had a value less than the mono-layer deposition case, which could be a strong point of patterned membranes rather than non-patterned membranes. So topological properties of the apex region of the surface patterns are shown to play an important role in anti-fouling.

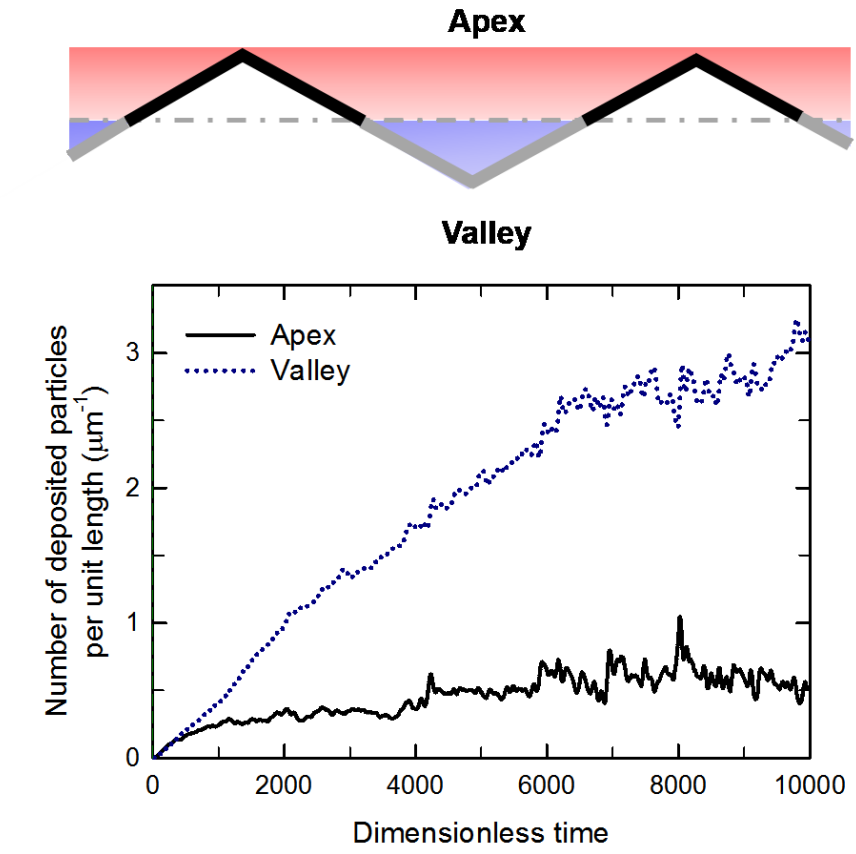

Figure 4.8. . Number of deposited colloidal particles per unit length counted in the area between surface patterns.

4.2.4. Implication on biofouling in the patterned membrane

Biological particles had not been considered in this study, however, dynamics of them near the patterned membrane surface could be related with the results from this study. Aggregating colloidal particles could form a particle cluster which might be thought as a microorganism. We could observe dynamics of particle clusters near the patterned membrane surface, and their movement were influenced by distorted flow field. In this context, dynamics of biological particles could be considered with the results from the experiment and simulation in this study.

It is inevitable to suffer from bio-fouling because the growth rate of microorganisms is surprisingly high. Even extremely small fraction of them in the feed solution could be led to huge population on the membrane surface. So it is crucial to detach microorganisms and extracellular polymeric substance (EPS) matrix secreted from them, not to focus on full prevention of their attachment. With the use of patterned membranes, high shear stress could be useful to detach microorganisms from the apex region of the membrane surface. In the valley region, where stagnant flow zone is induced, deposition of biological particles is relatively readable. But the mass transfer of nutrients which is crucial for the growth of microorganisms is limited to be transferred by diffusion because the flow in this area is almost stagnant. So it could be anticipated to control biofouling in the patterned membrane effectively with various topological properties of patterned membranes.

Chapter 5 Conclusion

Colloidal fouling on the patterned membrane was studied with cross-flow microfiltration experiment and Brownian dynamics simulation. To understand dynamics of buoyant particles near the patterned membrane surface, a model colloidal feed solution was prepared to conduct microfiltration experiment. We used dilute PMMA particle suspension. From the observation of fouled surface through scanning electron microscope (SEM), fouling behavior could be shown with difference in the apex region and the valley region. Non-fouled surface was shown in the apex region as time proceeded, and more particles were deposited toward the valley region. In the valley region, particles were continuously deposited onto the membrane surface.

Brownian dynamics simulation showed similar trend in colloidal fouling. Flow separation was induced between the valley area and bulk flow region by the presence of surface patterns. High wall shear stress was distributed around the apex region of the surface patterns and flow stagnant zone was shown in the valley region. Dynamics of particles in this flow environments could be tracked by Brownian dynamics simulation with a distorted flow field. Deposited particles in the apex region were shown to be swept by rapid mainstream and this was related to high wall shear stress distributed in this region. Dynamics of particles were affected by the permeation flux and attractive force of the membrane in the valley region. So particle dynamics near the patterned membrane could be understood with the flow characteristics around the membrane surface.

Reference

1. Global Footprint Network. What happens when an infinite-growth economy runs into a finite planet? U.S.A.: Global Footprint Network, 2012.

2. Wackernagel, M. et al. Our ecological footprint : reducing human impact on the earth. Canada: New Society Publishers, 1998.

3. Shannon, M.A. et al. "Science and technology for water purification in the coming decades." Nature 452(7185) (2008): 301-310.

4. World Health Organization. Global water supply and sanitation assessment 2000 report, Switzerland: World Health Organization, 2000.

5. Taylor, J.S. Assessment of potable water membrane applications and research needs. U.S.A.: American Water Works Association, 1989.

6. Nguyen, T., F. et al. "Biofouling of water treatment membranes: a review of the underlying causes, monitoring techniques and control measures." Membranes 2(4) (2012): 804-840.

7. Vogelaar, L. "Phase separation micromolding: a new generic approach for microstructuring various materials." Small 1(6) (2005): 645-655.

8. Petronis, S. "Design and microstructuring of PDMS surfaces for improved

marine biofouling resistance." J. Biomater. Sci. Polym. 11(10) (2000): 1051-72.

9. Chen, C.S. "Geometric control of cell life and death." Science 276(5317) (1997): 1425-8.

10. Çulfaz, P.Z. "Fouling behavior of microstructured hollow fiber membranes in dead-end filtrations: critical flux determination and NMR imaging of particle deposition." Langmuir 27(5) (2011): 1643-52.

11. Çulfaz, P.Z. "Microstructured hollow fibers for ultrafiltration." J. Memb. Sci. 347(1–2) (2010): 32-41.

12. Won, Y.J. "Preparation and application of patterned membranes for wastewater treatment." Environ Sci Technol. 46(20) (2012): 11021-7.

13. Lee, Y.K. "Flow analysis and fouling on the patterned membrane surface." J. Memb. Sci. 427 (2013): 320-325.

14. Satoh, A. Introduction to molecular-microsimulation of colloidal dispersions. The Netherlands: Elsevier, 2003.

15. Visser, J. "On Hamaker constants: a comparison between Hamaker constants and Lifshitz-van der Waals constants." Adv. Colloid Interface Sci. 3(4) (1972): 331-363.

16. Bhattacharjee et al. "Surface element integration: a novel technique for

evaluation of DLVO interaction between a particle and a flat plate." J. Colloid Interface Sci. 193(2) (1997): 273-285.

17. Goodwin, J.W. et al. "The relaxation spectrum and diffusion in concentrated systems of spherical particles." J. Chem. Phys. 95(8) (1991): 6124.

국문요약

패턴형 분리막에서의 막오염 매커니즘을 이해하기 위해 교차형 흐름 미세여과(microfiltration) 실험과 브라운 동역학 전산모사를 병행하였다. 상반전 기법(phase inversion technique)을 통해 분리막 표면에 가로 400μm, 세로 100μm의 미세한 프리즘 패턴을 전사하여 패턴형 분리막을 제조했다. 이 분리막에서의 부유물 오염 양상을 살펴보기 위해 PMMA 콜로이드 입자를 증류수에 잘 분산시킨 모델 유체를 이용하여 미세여과 실험을 수행했다. 일정 시간 동안 펌프를 통해 일정한 유속을 가하며 막오염 실험을 진행했고, 실험을 마친 후에는 분리막을 실험장치에서 꺼냈다. 그리고 주사 전자 현미경(SEM)을 이용하여 분리막 표면에 쌓여 있는 입자들을 관찰하였다. 입자는 주로 표면 패턴의 상단부 보다는 하단부 쪽에 많이 적층되어 있었고, 상단부에는 실험 시작 이후 시간이 경과하였음에도 입자가 전혀 쌓여 있지 않은 영역이 확인되기도 하였다. 이렇게 패턴형 분리막의 상단부와 하단부에서의 입자 적층 양상의 차이는 표면 패턴 주변의 유동 특성 연관될 것이라 생각되었다.

수치해석을 통해 패턴형 분리막 주변의 교란된 유동장을 계산하였고, 이를 이용하여 콜로이드 입자의 움직임을 계산할 수 있었다. 유동 계산 결과에서 표면 패턴 주변에는 교차형 흐름기 내의 유동과 분리되는 매우 느린 유동이 발생하였고, 표면 패턴의 상단부에는 유동에 의해 전단 응력이 매우 크게 형성되어 있었다. 브라운 동역학 전산모사는 이러한 유동 특성이 반영되어 수행되었고, 입자는 패턴형 분리막의 상, 하단부에서 다르게 거동하였다. 분리막의 상단부에서는 입자가 분리막 표면에서 강한 전단 응력을 받아 쉽게 떨어져 나가는 모습이 관찰되었고, 이 영역에서 입자는 잘 쌓이지 못했다. 반면 분리막의 하단부에서는 입자가 느린 유동 영역에 진입하게 될 경우, 교차 흐름의 영향을 거의

받지 못하고 분리막 쪽으로의 투수 유속과 분리막 표면이 입자에게 가하는 인력의 영향을 받아 분리막 표면에 쉽게 쌓였다. 이로 인해 분리막 하단부에서는 상단부에서보다 막오염이 빠르게 일어났다.

이러한 거동은 실제 처리수에 포함되어 있는 미생물 등의 부유물에 대해서도 일어날 수 있을 것으로 예상할 수 있다. 본 연구 결과가 보다 개선된 패턴형 분리막을 설계하는 데에 기여할 수 있을 것으로 기대한다.